Systematic behavior of mass distributions in ^{48}Ti-induced fission at near-barrier energies

C. J. Lin,[1,2,*] R. du Rietz,[1] D. J. Hinde,[1] M. Dasgupta,[1] R. G. Thomas,[1,†] M. L. Brown,[1,‡] M. Evers,[1] L. R. Gasques,[1,§] and M. D. Rodriguez[1,‖]

[1]*Department of Nuclear Physics, Research School of Physics and Engineering, The Australian National University, Canberra, ACT 0200, Australia*

[2]*China Institute of Atomic Energy, P. O. Box 275(10), Beijing 102413, China.*

(Received 18 December 2011; published 19 January 2012)

The mass distributions of the fission fragments were measured in reactions induced by ^{48}Ti beams on ^{144,154}Sm, ^{162}Dy, ^{174}Yb, ^{186}W, ^{192}Os, ^{196}Pt, ^{200}Hg, and ^{208}Pb targets at near-barrier energies. The systematic tendencies of the mass widths have been explored. For the reactions with the lighter or spherical target nuclei, the mass widths increase with increasing bombarding energy, a behavior expected for fusion-fission. For the heavier and statically deformed nuclei, the mass widths increase rapidly as energies fall close to and below the capture barriers. Well above the barrier energies, the mass widths and estimated minimum quasifission contributions increase smoothly with increasing fissility of the composite nucleus. The observed behavior is a complex function of the fissility, deformation, and energy with respect to the capture barrier. Comparisons with dynamical quasifission model calculations for these reactions will be a good test of models of fusion in heavy-element formation reactions.

DOI: 10.1103/PhysRevC.85.014611 PACS number(s): 25.70.Jj, 25.70.Gh, 25.85.Ge

I. INTRODUCTION

Heavy-ion-induced fission is a complicated dynamical process in which many degrees of freedom are intimately involved, as a nucleus is first formed and then splits into two. Although qualitative and sometimes quantitative descriptions of many aspects of the process have been achieved, as yet it is not completely understood. A fundamental property of fission is the mass-split or the distribution of mass-splits that arises from an ensemble of fissioning nuclei. In low-energy fission of actinide elements, the mass-splits are not centered on symmetry, resulting in the well-known mass-asymmetric fission. However, at higher excitation energies, such as in heavy-ion-induced fusion-fission (FF), this generally transforms to fission peaked at mass symmetry, as is also found for lighter nuclei. The transition to mass symmetry is understood to be due to the washing out of shell effects in the level densities with increasing excitation energy. The simplest way to model FF is to assume that all degrees of freedom (including the mass degree of freedom) achieve their equilibrium statistical values, generally those associated with the fission saddle point [1–3]. However, it has been recognized that they may be modified during the descent from the fission saddle point to scission point, and recent dynamical calculations suggest that this effect can be significant [4].

The mass distributions for FF have often been calculated on the basis of equilibrium statistical properties of the nucleus. This requires knowledge of the average nuclear temperature, mean spin, moments of inertia, and stiffness of the potential against mass-asymmetric perturbations, generally at the fission saddle point. Calculations have also been carried out at the scission point [5,6]. Many of these input quantities can be provided by the macroscopic liquid-drop model [7,8]. The calculated fission characteristics at the saddle point and/or scission point have been used [9,10] as a reference to assess whether a given reaction actually proceeds via the FF process.

Such comparisons have shown [9–13] that in heavy-ion reactions forming very heavy elements, another class of fission is present, called quasifission (QF), which is understood to be a rapid dynamical process, in which many degrees of freedom do not reach their equilibrium distributions. The rapid time scale is associated with the failure to reach a compact compound nucleus shape. The mass degree of freedom has been a central criterion [14] used to identify the presence of quasifission when admixed with FF. In reactions where QF is believed to be present, the width of the fragment mass distribution is greater than that for FF. This is because the mass degree of freedom fails to achieve complete relaxation, in other words, there is a memory of the masses of the projectile and target nuclei. Hence, an increased mass width is used as an indicator of the presence of QF [15].

In reactions showing broad mass distributions, measured mass-angle distributions [12,13,16,17] have shown a correlation of fragment mass with angle. This observation indicates that the dinuclear system, when splitting into two mass-asymmetric fragments, has a memory of projectile mass and direction. The observation of a mass-angle correlation is inconsistent with the formation of an equilibrated compound nucleus. Therefore, the asymmetric fragments cannot be from equilibrium FF but must be from incompletely relaxed reactions of the projectile and target, with reaction time scales typically less than the rotation time of the composite system [11–13,16–18].

*cjlin@ciae.ac.cn

†Present address: Nuclear Physics Division, Bhabha Atomic Research Centre, Mumbai 400085, India.

‡Present address: Navman NZ Ltd., 7-11 Kawana St, Northcote, Auckland, New Zealand.

§Present address: Laboratório Pelletron, Instituto de Física da Universidade de São Paulo, 05315-970, São Paulo, SP, Brazil.

‖Present address: Department of Electronic Materials Engineering, RSPE, ANU, ACT 0200, Australia.

QF becomes probable when the projectile mass and/or the product of the charges of projectile and target increases above a certain threshold, whose values are not yet well established. Through investigation of different reactions forming the same compound nucleus, it was found that QF rapidly becomes more probable for reactions with increasing mass symmetry [16,19,20]. Experimentally it is also found that the fissility of the compound nucleus, which determines the saddle-point shape and fission barrier [21], has an important influence on the measured mass distribution.

However, questions still remain about the dependence of the probability and characteristics of QF on the beam energy with respect to the capture barrier. For fission induced by light projectiles, systematic studies [22] showed that the mass widths basically follow a decreasing trend with decreasing energy for a given system [23,24]. For fission following reactions with heavier projectiles, the systematic tendency is not so clear. Back *et al.* [16] found that the mass widths basically decrease with decreasing bombarding energy. However, Shen *et al.* [13] observed the mass widths for the reactions of ^{32}S and ^{35}Cl with ^{238}U were larger at the lowest energy than those at higher energies. Recent measurements [17,25], taken with small energy steps, showed that for reactions with heavy, statically deformed nuclei, the mass widths can increase rapidly as the bombarding energy drops through the region of the capture barrier energy. This effect has been interpreted [17,23,26] as showing that the mass width depends strongly on the angle between the nuclear deformation axis and the contact point of the lighter nucleus (referred to as deformation alignment).

In this work, a systematic investigation was performed on the mass distributions of the fission events following reactions of ^{48}Ti beams with targets ranging from ^{144}Sm to ^{208}Pb to probe the competition between the influence of nuclear deformation alignment and fissility of the composite nucleus.

II. EXPERIMENTAL METHOD

The experiments were carried out at the Heavy Ion Accelerator Facility at the Australian National University, using ^{48}Ti pulsed beams with a typical pulse width of ∼1.5 ns and separation of 106.7 ns. Energies ranged from 0.98 to 1.3 times the capture barrier energies, corresponding to an energy range of 206 to 296 MeV. Energies up to 245 MeV were provided by the 14UD tandem electrostatic accelerator, and higher energies utilized the superconducting linear booster accelerator. These beams bombarded isotopically enriched targets of ^{144}Sm (∼55 μg/cm^2), ^{154}Sm (∼30 μg/cm^2), ^{162}Dy (∼30 μg/cm^2), ^{174}Yb (∼64 μg/cm^2), ^{186}W (∼52 μg/cm^2), ^{192}Os (∼100 μg/cm^2), ^{196}Pt (∼53 μg/cm^2), ^{200}Hg (∼30 μg/cm^2), and ^{208}Pb (∼80 μg/cm^2). Targets were supported by ∼15 μg/cm^2 C backings (facing downstream) and oriented with their normal at 60° to the beam direction. Fission fragments were detected in coincidence in two large-area (284 × 357 mm^2) multiwire proportional counters (MWPCs). The forward angle detector was centered at $\theta_{\rm lab} = 45°$ with 4°–81° coverage, the backward angle detector being centered at 90° with 50°–126° coverage. The position and timing information from the two MWPCs was utilized to determine the velocity vectors of the two particles on an event-by-event basis and to deduce [23] the ratio of the mass of one fragment to the sum of two fragments, i.e., $M_R = M_{\rm Back}/(M_{\rm Back} + M_{\rm Front})$. This relationship relies on the assumption that neutron evaporation does not change the fragment velocity on average. The fragment mass was derived by $M = M_R M_{\rm CN}$ with the assumption that $M_{\rm CN} = M_{\rm Back} + M_{\rm Front}$, where $M_{\rm CN}$ indicates the mass of compound nucleus. Neutron evaporation is, thus, neglected. A gate on the spectrum of parallel velocity versus perpendicular velocity of the composite system was applied to suppress random coincidences as well as reject background reactions [23]. Further details of the experimental setup and the analysis procedure can be found in Refs. [17,20,23,25,26].

III. EXPERIMENTAL MASS WIDTHS

To present the experimental data from ∼50 separate measurements, it is desirable to find an appropriate parametrization of the experimental results. Since the focus of this work is on overall mass widths, the mass spectra measured over a center-of-mass angular range of ∼40° to ∼140° were consolidated into a single mass spectrum associated with the whole angular range accessible to the experiment. Typical

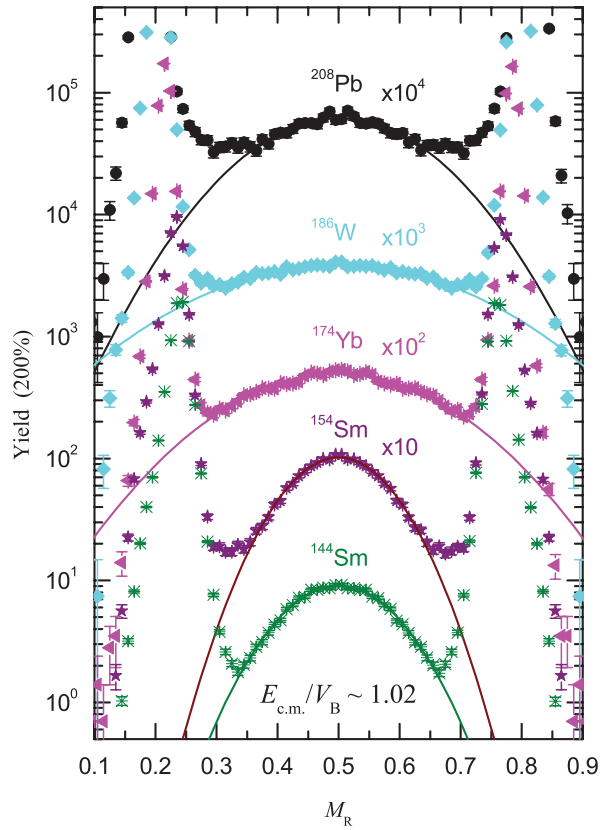

FIG. 1. (Color online) Mass-ratio distributions and their Gaussian fits for ^{48}Ti + ^{208}Pb, ^{186}W, ^{174}Yb, ^{154}Sm, and ^{144}Sm systems, respectively, at $E_{\rm c.m.}/V_B$ ∼ 1.02. Fission yields are normalized to 200% based on the fits.

M_R spectra are shown in Fig. 1, for ^{48}Ti beam energies corresponding to ∼1.02 times the respective capture barrier energies, for the indicated target nuclei. The capture barriers were calculated from the work of Ref. [27]. It should be noted that the spectra shown are specific to the angular range of the measurement. Neglecting possible structure in the mass spectra seen at the lowest energies for a few reactions [25], possibly induced by shell effects, the mass distributions were all reproduced reasonably well, or very well, by adjusting the width of a Gaussian function. In order to avoid distortion by the deep-inelastic scattering events at both sides, only the center regions, corresponding to $M_R = 0.36$–0.64, were fitted for all the distributions.

The mass widths give a compact representation of the very extensive data set, which allows an investigation of whether the trends of the data can be described systematically by one parameter or a few parameters. Those parameters providing a good ordering of the data should indicate the key physics defining the process.

A. Dependence on excitation energy

We first investigate the correlation of the mass widths with excitation energy (E_x). The latter is related to the nuclear temperature T by $T = (E_x/a)^{1/2}$, where a is the level density parameter, which may differ for different shape configurations. The standard deviations of the Gaussian fit function, i.e., mass width σ_M, are plotted as a function of the excitation energy of the compound nucleus, E_x, the excitation energy at the saddle point, $E_x^{\rm sad}$, and at the scission point, $E_x^{\rm sci}$ in Figs. 2(a)–2(c), respectively. Data from the literature for the ^{48}Ti + ^{166,170}Er reactions [16,25] are also included, indicated by the open symbols. Before discussing the observed behavior, we define how the various excitation energies were determined.

The excitation energy of the compound nucleus is calculated by

$$E_x = E_{\rm c.m.} + Q_{\rm fus}, \tag{1}$$

where $E_{\rm c.m.}$ is the center-of-mass energy and $Q_{\rm fus}$ is the fusion Q value calculated using ground-state masses. The excitation energy at the saddle point is defined as

$$E_x^{\rm sad} = E_x - B_f - E_{\rm pre}^{\rm sad} - E_{\rm rot}^{\rm sad}, \tag{2}$$

where B_f is the fission barrier height, $E_{\rm pre}^{\rm sad}$ is the energy carried away by presaddle neutron emission, and $E_{\rm rot}^{\rm sad}$ is the rotational energy at the saddle point. Unfortunately, there is no information on the presaddle neutron emission multiplicity. This was set to be half of that of the estimated prescission neutron emission [28]. B_f and $E_{\rm rot}^{\rm sad}$, which are related to the total spin of compound nucleus, were calculated by the rotating-liquid-drop model [8]. B_f values at zero spin were corrected according to the calculations of P. Möller *et al.* [29]. To determine the total spin of the compound nucleus, calculations were carried out using the CCFULL code [30], assuming the angular momentum in the capture channel is fully transferred to the combined system. In the CCFULL calculations, the deformation of the projectile and target nuclei were taken into account. The deformation parameters used were deduced by the corresponding reduced electromagnetic transition probabilities given in the ENSDF library [31]. The excitation energy at the scission point is determined from

$$E_x^{\rm sci} = E_x + Q_{\rm sym} - T_{\rm KE} - E_{\rm pre}^{\rm sci} - E_{\rm rot}^{\rm sci} - E_{\rm def}, \tag{3}$$

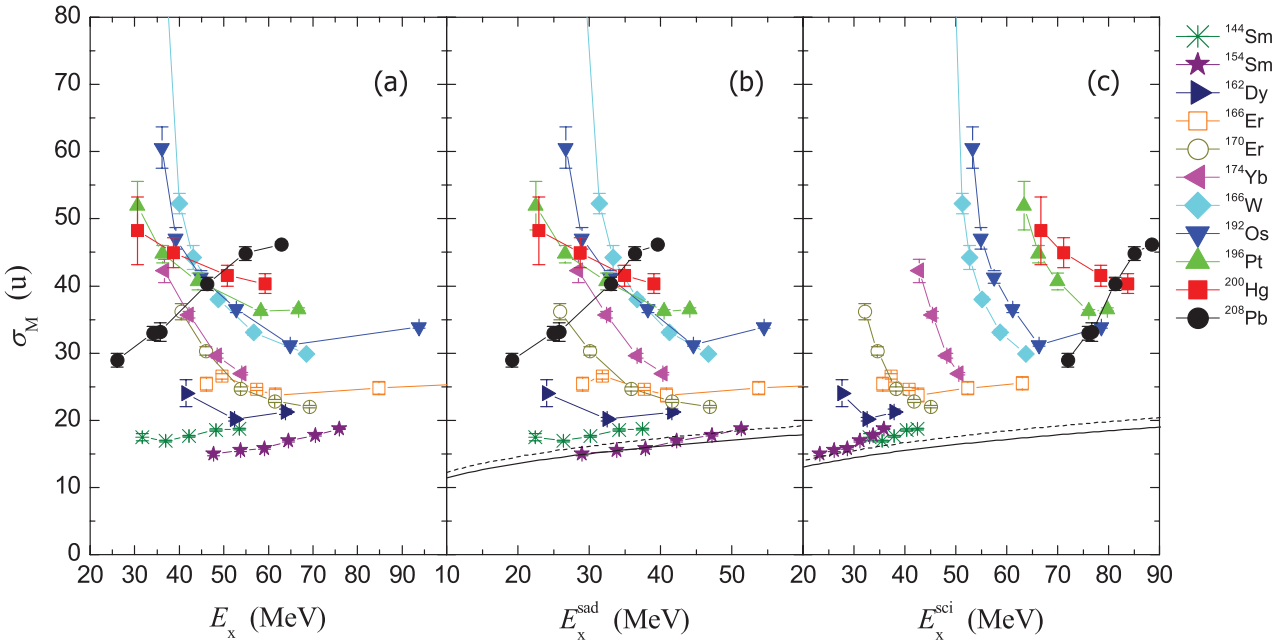

FIG. 2. (Color online) Mass widths are shown as the functions of (a) the excitation energy of compound nucleus (E_x), (b) the excitation energy at saddle point ($E_x^{\rm sad}$), and (c) the excitation energy at scission point ($E_x^{\rm sci}$). The error bars only represent the fitting errors. The estimations of the saddle-point and scission-point models for ^{144}Sm (dashed curves) and ^{208}Pb (solid curves) are also plotted in panels (b) and (c). The symbols identifying the target nucleus for each reaction keep their meaning for Figs. 3–6.

where $Q_{\rm sym}$ is the Q value for symmetric fission of the compound nucleus and $T_{\rm KE}$ is the most probable total kinetic energy released in fission [32]. $E^{\rm sci}_{\rm pre}$ is the energy carried away by prescission neutron emission, which was estimated using a prescission neutron multiplicity [33] multiplied by an assumed 8 MeV removed by each neutron. $E^{\rm sci}_{\rm rot}$ is the rotational energy at the scission point [34], and $E_{\rm def}$ is the deformation energy at the scission point which was set to 12 MeV, a value used for actinide nucleus fission [35].

Looking at the figure from Figs. 2(a) to 2(c) one can see that the tendencies of the mass width are rather haphazard as a function of E_x and $E^{\rm sad}_x$ but seem to show a more orderly arrangement as a function of $E^{\rm sci}_x$. This more orderly appearance is related to the increase in the excitation energy gain from saddle to scission, as the fissility (correlated with target nucleus atomic number) increases. Thus the data from one reaction are separated from the next in $E^{\rm sci}_x$, giving a less cluttered appearance. However, as might be imagined, the trends of the measurements with $E^{\rm sci}_x$ by no means match the predictions of the scission-point model [5,6], as shown below.

Assuming the mass-asymmetry driving potential can be approximated by a parabolic shape, the scission-point model mass width has been estimated by

$$\sigma_M^2 = \frac{T}{k} = \frac{1}{k}\sqrt{\frac{E_x}{a}}, \tag{4}$$

where T is the nuclear temperature at the scission point $T^{\rm sci}$ and k is the stiffness parameter, set to 0.0048 MeV/u^2 as in Ref. [16]. The scission-point temperature is determined from $E^{\rm sci}_x$ using a level density parameter $a = A/8.5\ {\rm MeV}^{-1}$, where A is the compound nucleus mass number. These scission-point model calculations for the reactions of ^{48}Ti with ^{144}Sm and ^{208}Pb are shown by the dashed and solid lines, respectively, in Fig. 2(c). Although the scission-point calculations reproduce the experimental data for the lightest targets (^{144,154}Sm) quite well, they fail quantitatively for all other reactions. A similar estimation of the expected equilibrium mass width has been made for the saddle-point conditions, calculating $T^{\rm sad}$ using $E^{\rm sad}_x$ and $a = A/10\ {\rm MeV}^{-1}$, which are shown in Fig. 2(b) for the targets of ^{144}Sm (dashed line) and ^{208}Pb (solid line). The discrepancy is similar for the scission-point calculations. This discrepancy must be attributed to QF.

B. Dependence on E/V_B

As noted in the Introduction, the orientation of statically deformed nuclei has previously been proposed [23,26] as an important variable in determining the competition between FF and QF. The orientations which can result in capture of the projectile nucleus in turn depend on the beam energy with respect to the average capture barrier [36]. At the lowest energy, only alignment of the longest axis of the deformed nucleus with the projectile direction can lead to capture, while well above the barrier, all orientations can be reached.

Accordingly, the mass widths σ_M for all reactions are plotted as a function of $E_{\rm c.m.}/V_B$ in Fig. 3. From this plot one can recognize that the trends of σ_M versus $E_{\rm c.m.}/V_B$ for the spherical ^{144}Sm and ^{208}Pb targets differ markedly from those

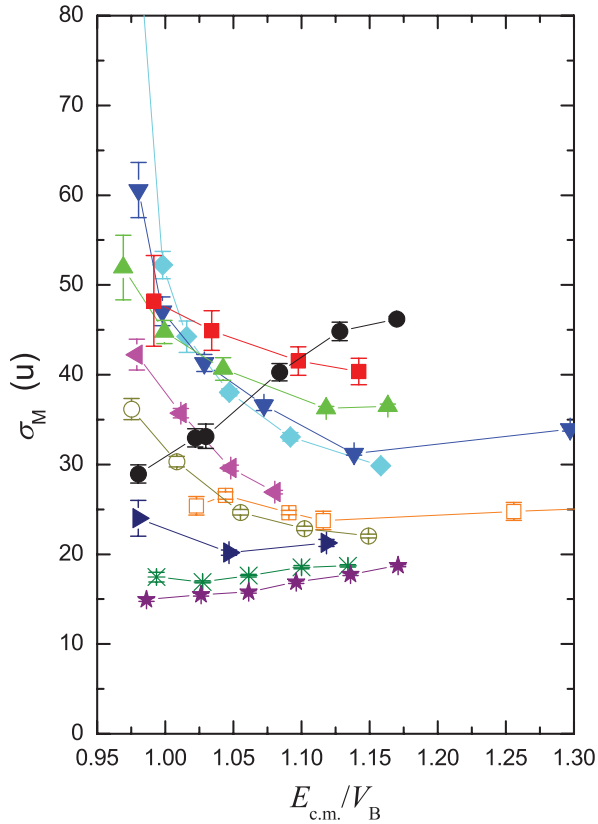

FIG. 3. (Color online) The mass widths of the fission fragments are shown as a function of the center-of-mass energy with respect to the capture barrier for each reaction.

of the others. For ^{144}Sm and ^{208}Pb, the mass widths uniformly increase as the beam energy increases from below the average capture barrier energy to well above. For all the other reactions, an increase with energy is found only at energies well above the barrier. When the reaction energies are close to or below the barrier, $E_{\rm c.m.}/V_B < 1.1$, the mass widths instead increase with *decreasing* energy. As noted above, this can be correlated with the different probability and characteristics of QF associated with the collisions on the tips of the deformed target nuclei. Even the reaction with the light but deformed ^{154}Sm target nucleus shows a small but significant rise in σ_M at subbarrier energies [20].

Thus, the strong increase in the σ_M subbarrier flags the importance to the reaction outcome of the alignment of the long axis of the statically deformed heavy reaction partner with respect to the beam direction.

C. Dependence on fissility

By focusing on the fission characteristics above the capture barrier energy region, the observed fission events will result from an average over all orientations and, thus, should be minimally sensitive to the size (and alignment) of the static deformation. This allows the influence of the fissility of the composite system being formed to be investigated most clearly. The mass widths at $E_{\rm c.m.}/V_B = 1.15$ were used to study the systematic dependence of σ_M with fissility. Because of the

extensive data set, measurements for most of the reactions were available on either side or very close to this value of $E_{c.m.}/V_B$. Thus, the mass widths and their uncertainties could be derived by interpolation or slight extrapolation. The only exception is the ^{48}Ti + ^{174}Yb reaction, where the mass width at the highest measured energy ($E_{c.m.}/V_B = 1.08$) was used.

The systematic behavior of σ_M versus the fissility [21] of the composite nucleus is illustrated in Fig. 4, for $E_{c.m.}/V_B = 1.15$ and also for $E_{c.m.}/V_B = 0.99$. Saddle-point and scission-point model calculations are indicated by the dotted and dashed curves, respectively. As expected from previous figures, they do not predict the behavior seen experimentally. The subbarrier data do not show a monotonic increase with fissility but increase rapidly up to fissility 0.821 (^{48}Ti + ^{186}W), then decrease as far as 0.886, corresponding to the ^{48}Ti + ^{208}Pb reaction. This can be correlated with the decrease in static deformation from ^{186}W to ^{208}Pb (spherical). In contrast, the above-barrier data show a smooth monotonic increase with fissility. The comparison with the subbarrier mass widths brings out an important point: The deviations from a smooth increase seen below-barrier are completely absent above-barrier. This is emphasized by the very small deviations of the experimental $E_{c.m.}/V_B = 1.15$ mass widths from an exponential fit to the data. This indicates that effects of deformation alignment, very prominent at subbarrier energies, have been averaged out in the above-barrier fission mass distributions, where all orientations contribute to capture.

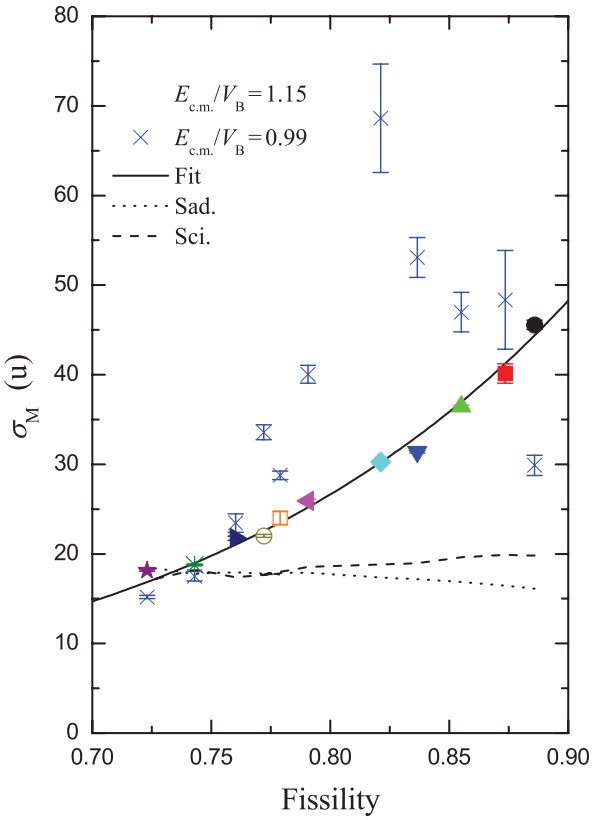

FIG. 4. (Color online) Mass widths are shown as a function of the fissility of the composite nucleus at $E_{c.m.}/V_B = 1.15$ (target symbols) and at $E_{c.m.}/V_B = 0.99$ (blue crosses). The exponential fit to the $E_{c.m.}/V_B = 1.15$ data emphasizes the smooth behavior of the above-barrier data compared with the structure seen in the below-barrier data. The calculations with the saddle-point model (dotted curves) and scission-point model (dashed curves) are also shown.

D. Estimation of quasifission probability

FF in heavy-ion reactions shows the peak yield at mass-symmetric splits and a narrow mass distribution. If the mass width expected for FF in each reaction can be predicted, then the mass spectra can be used to estimate the minimum fraction attributed to QF. This makes use of the assumption that the yield at symmetry is attributed completely to FF. It is unlikely that QF makes no contribution to the observed mass-symmetric events. This makes the QF probability extracted in this way a lower limit.

Using the scission-point model presented previously (Sec. III A) to predict the mass width for FF, the minimum proportion of QF can be determined according to the expression $P(\mathrm{QF})_{\min} = 1 - \sigma_M^{\mathrm{sci}}/\sigma_M^{\mathrm{exp}}$, where σ_M^{sci} and σ_M^{exp} are, respectively, the theoretical and experimental Gaussian widths of the mass spectra. The dependence of $P(\mathrm{QF})_{\min}$ on fissility is shown in Fig. 5. Note that if σ_M^{exp} is very large, significant yield can be attributed to unphysical masses, thus, the largest values of $P(\mathrm{QF})_{\min}$ should be treated with caution and should be considered to show indicative trends. For $E_{c.m.}/V_B = 1.15$, $P(\mathrm{QF})_{\min}$ increases linearly from ~0.05

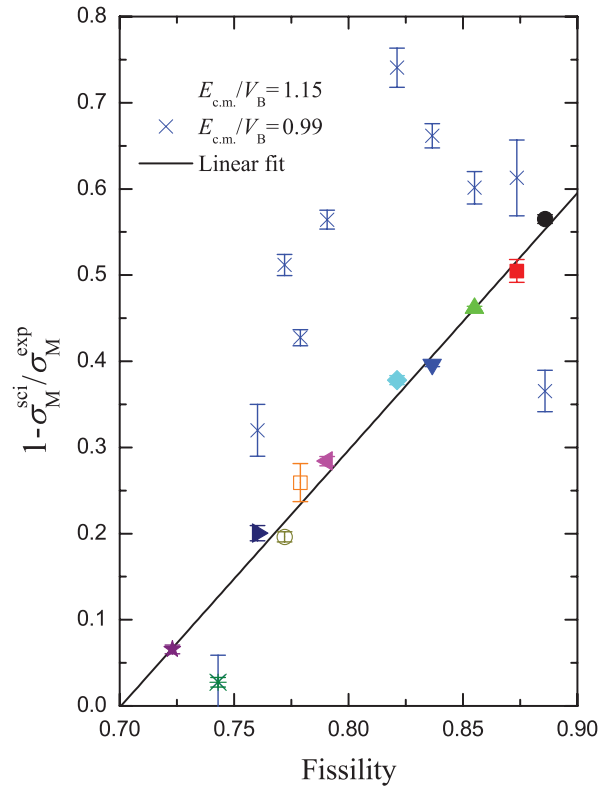

FIG. 5. (Color online) The estimated minimum fraction of QF (see text) at $E_{c.m.}/V_B = 1.15$ (target symbols), with linear fit (solid line), plotted as a function of fissility. Results at $E_{c.m.}/V_B = 0.99$ (blue crosses) are also shown for comparison.

for ^{48}Ti + ^{154}Sm, to 0.57 for the ^{48}Ti + ^{208}Pb reaction. The error bars on the data points arise only from the experimental uncertainties in the mass widths; uncertainties in the reference calculations for FF are not considered.

The same analysis procedure was applied to the mass widths from below-barrier energies corresponding to $E_{\rm c.m.}/V_B = 0.99$, indicated by the blue crosses in Fig. 5. Here we expect to see the sensitivity to the heavy reaction partner's static deformation. Indeed, it is clearly seen that the QF probability increases, associated with the deformation effects for most of the systems, but is reduced for the reaction with the spherical ^{208}Pb.

E. Correlation of subbarrier σ_M with deformation

In order to isolate the effects of deformation at energies below the average capture barrier, a mass-width enhancement factor was introduced, defined as $\sigma_M(E_x^{\rm sci})^{1/4}/[\sigma_M(E_x^{\rm sci})^{1/4}]_{E_{\rm ref}}$, where $E_{\rm c.m.}/V_B = 1.15$ was taken as reference. The effect of the E_x scaling is small, between 4.5% and 10%, and may, to first order, compensate for the different excitation energies at different $E_{\rm c.m.}/V_B$. Figure 6 displays the relationship between the enhancement factor and the deformation parameter β_2 at energies corresponding to $E_{\rm c.m.}/V_B = 0.99$ for each reaction. For the systems with fissility greater than 0.8, associated with target nuclei with deformations $\beta_2 \leqslant 0.24$, the enhancement factors show a linear dependence on the deformation parameter. As deformation has been shown to be an important variable in determining the mass width in QF, an increase in deformation would be expected to increase the mass width in reactions where QF is dominant. This linear increase does not hold for the less fissile systems, where, despite having $\beta_2 > 0.24$, the enhancement factor depends much less on β_2. This rapid change in behavior must reflect the reduced QF probabilities for these reactions forming composite nuclei with lower fissilities. In principle, this gives information on the detailed balance between fissility and deformation in defining the dynamics and, thus, QF probabilities. A quantitative description of the systematic behavior revealed in this study will be a challenge for theoretical models of the competition between FF and QF.

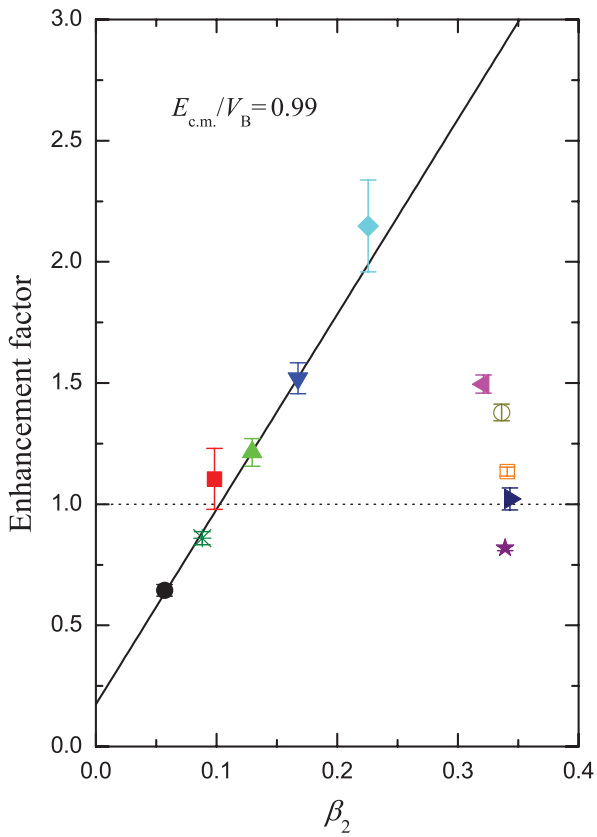

FIG. 6. (Color online) The mass-width enhancement factors at energies corresponding to $E_{\rm c.m.}/V_B = 0.99$ as a function of the deformation parameter. The linear fit describes only the results for the reactions with the smaller β_2 values.

IV. SUMMARY AND CONCLUSIONS

In summary, the mass distributions of the fission fragments have been measured in reactions induced by ^{48}Ti beams on ^{144,154}Sm, ^{162}Dy, ^{174}Yb, ^{186}W, ^{192}Os, ^{196}Pt, ^{200}Hg, and ^{208}Pb targets at beam energies near and below the energies of the capture barriers. The distributions are generally well represented by Gaussian functions. The systematic trends of the mass widths have been investigated as a function of the excitation energy of the compound nucleus, the excitation energy at the saddle point, and at the scission point. The mass widths do not show uniform systematic behavior as a function of any of these variables. The mass distributions are generally much wider than equilibrium mass distributions calculated for the saddle point or scission point, indicating the presence of a substantial contribution from QF. The mass widths for many of the reactions show a consistent systematic trend as a function of the bombarding energy with respect to the capture barrier, with the widest distributions at the lowest energies. Exceptions are reactions with the spherical target nuclei, where the mass widths increase monotonically with energy from the lowest measured beam energies. These systematic trends indicate that mass distributions are very wide (showing the presence of QF and short reaction time scales) for those collisions making contact with the elongated tips of the statically deformed heavy reaction partners, which are the only orientations leading to capture at the lowest beam energies. At energies well above the capture barriers, the mass widths exhibit a smooth dependence on the fissility of the composite system. Estimations of the minimum probability of QF show a linear dependence on the fissility. Thus, it is concluded that the observed behavior is a function of the fissility, static deformation, and bombarding energy with respect to the capture barrier. The systematic study presented here, when compared with model calculations, should lead to a better understand of the dynamics of QF, which is the main competitor to fusion in reactions forming very heavy and superheavy nuclei.

ACKNOWLEDGMENTS

The authors acknowledge ARC support through Discovery Grants No. DP0664077 and No. DP110102858. C. J. Lin thanks the NSFC for partial support under Grants No. 10735100 and No. 10975192.

[1] A. Bohr, in *Proceedings of the United Nations International Conference on the Peaceful Uses of Atomic Energy, Geneva, 1955* (United Nations, New York, 1956).
[2] I. Halpern and V. M. Strutinsky, in *Proceedings of the Second United Nations International Conference on the Peaceful Uses of Atomic Energy, Geneva, 1958* (United Nations, Geneva, Switzerland, 1958).
[3] R. Vandenbosch and J. R. Huizenga, *Nuclear Fission* (Academic Press, New York, 1973).
[4] A. V. Karpov, R. M. Hiryanov, A. V. Sagdeev, and G. D. Adeev, J. Phys. G **34**, 255 (2007).
[5] P. D. Bond, Phys. Rev. Lett. **52**, 414 (1984).
[6] H. H. Rossner, J. R. Huizenga, and W. U. Schröder, Phys. Rev. Lett. **53**, 38 (1984).
[7] J. R. Nix and W. J. Swiatecki, Nucl. Phys. **71**, 1 (1965).
[8] A. J. Sierk, Phys. Rev. C **33**, 2039 (1986).
[9] B. B. Back, R. R. Betts, K. Cassidy, B. G. Glagola, J. E. Gindler, L. E. Glendenin, and B. D. Wilkins, Phys. Rev. Lett. **50**, 818 (1983).
[10] D. J. Hinde, C. R. Morton, M. Dasgupta, J. R. Leigh, J. C. Mein, and H. Timmers, Nucl. Phys. A **592**, 271 (1995).
[11] R. Bock *et al.*, Nucl. Phys. A **388**, 334 (1982).
[12] J. Tōke *et al.*, Nucl. Phys. A **440**, 327 (1985).
[13] W. Q. Shen *et al.*, Phys. Rev. C **36**, 115 (1987).
[14] M. B. Tsang, D. Ardouin, C. K. Gelbke, W. G. Lynch, Z. R. Xu, B. B. Back, R. Betts, S. Saini, P. A. Baisden, and M. A. McMahan, Phys. Rev. C **28**, 747 (1983).
[15] G. N. Knyazheva *et al.*, Phys. Rev. C **75**, 064602 (2007).
[16] B. B. Back, P. B. Fernandez, B. G. Glagola, D. Henderson, S. Kaufman, J. G. Keller, S. J. Sanders, F. Videbæk, T. F. Wang, and B. D. Wilkins, Phys. Rev. C **53**, 1734 (1996).
[17] D. J. Hinde, R. G. Thomas, R. du Rietz, A. Diaz-Torres, M. Dasgupta, M. L. Brown, M. Evers, L. R. Gasques, R. Rafiei, and M. D. Rodriguez, Phys. Rev. Lett. **100**, 202701 (2008).
[18] R. du Rietz, D. J. Hinde, M. Dasgupta, R. G. Thomas, L. R. Gasques, M. Evers, N. Lobanov, and A. Wakhle, Phys. Rev. Lett. **106**, 052701 (2011).
[19] A. C. Berriman, D. J. Hinde, M. Dasgupta, C. R. Morton, R. D. Butt, and J. O. Newton, Nature (London) **413**, 144 (2001).
[20] R. Rafiei, R. G. Thomas, D. J. Hinde, M. Dasgupta, C. R. Morton, L. R. Gasques, M. L. Brown, and M. D. Rodriguez, Phys. Rev. C **77**, 024606 (2008).
[21] B. B. Back, R. R. Betts, J. E. Gindler, B. D. Wilkins, S. Saini, M. B. Tsang, C. K. Gelbke, W. G. Lynch, M. A. McMahan, and P. A. Baisden, Phys. Rev C **32**, 195 (1985).
[22] Y. S. Sawant, A. Saxena, R. K. Choudhury, P. K. Sahu, R. G. Thomas, L. M. Pant, B. K. Nayak, and D. C. Biswas, Phys. Rev. C **70**, 051602(R) (2004).
[23] D. J. Hinde, M. Dasgupta, J. R. Leigh, J. C. Mein, C. R. Morton, J. O. Newton, and H. Timmers, Phys. Rev. C **53**, 1290 (1996).
[24] R. Yanez, D. J. Hinde, B. Bouriquet, and D. Duniec, Phys. Rev. C **71**, 041602(R) (2005).
[25] R. G. Thomas, D. J. Hinde, D. Duniec, F. Zenke, M. Dasgupta, M. L. Brown, M. Evers, L. R. Gasques, M. D. Rodriguez, and A. Diaz-Torres, Phys. Rev. C **77**, 034610 (2008).
[26] D. J. Hinde, M. Dasgupta, J. R. Leigh, J. P. Lestone, J. C. Mein, C. R. Morton, J. O. Newton, and H. Timmers, Phys. Rev. Lett. **74**, 1295 (1995).
[27] W. J. Swiatecki, K. Siwek-Wilczynska, and J. Wilczynski, Phys. Rev. C **71**, 014602 (2005).
[28] J. P. Lestone, A. A. Sonzogni, M. P. Kelly, and R. Vandenbosch, Phys. Rev. C **56**, R2907 (1997).
[29] P. Möller, A. J. Sierk, T. Ichikawa, A. Iwamoto, R. Bengtsson, H. Uhrenholt, and S. Aberg, Phys. Rev. C **79**, 064304 (2009).
[30] K. Hagino, N. Rowley, and A. T. Kruppa, Comput. Phys. Commun. **123**, 143 (1999).
[31] [http://www.nndc.bnl.gov/ensdf/].
[32] V. E. Viola, K. Kwiatkowski, and M. Walker, Phys. Rev. C **31**, 1550 (1985).
[33] D. Hilscher and H. Rossner, Ann. Phys. Fr. **17**, 471 (1992).
[34] M. G. Itkis and A. Ya. Rusanov, Phys. Part. Nuclei **29**, 160 (1998).
[35] B. B. Back, Phys. Rev. C **31**, 2104 (1985).
[36] M. Dasgupta, D. J. Hinde, N. Rowley, and A. M. Stefanini, Annu. Rev. Nucl. Part. Sci. **48**, 401 (1998).